

# FOLIAGEN: FRAMEWORK FOR FOLIAGE IMAGE GENERATION FROM INDIVIDUAL CROP LEAF IMAGES

## Anonymous authors

Paper under double-blind review

## ABSTRACT

While machine learning (ML)-based crop disease classifiers mostly targeted individual leaf images, real-world applications call for disease classification on crop foliage images instead, because they usually rely on cameras mounted on unmanned aerial vehicles to capture foliage images across vast crop fields for automated disease identification. We found that known state-of-the-art (SOTA) classifiers on the only real-world soybean foliage image dataset all exhibited unsatisfactory performance, despite the dataset being modest-sized and including just two soybean disease categories (among many). Hence, it is desirable to make available large foliage image datasets with common crop disease categories for better evaluating and possibly improving SOTA crop disease classifiers on foliage images. This paper introduces a framework that generates crop foliage images utilizing available datasets of individual leaf images, termed Foliagen (short for foliage generation). A generated foliage image dataset can be arbitrarily sized, with each image emulating the natural distribution of diseased leaves with a specified disease rate. Being annotated by design, such generated datasets are valuable for (1) evaluating the SOTA classifiers when applied to practical use and (2) pre-training general SOTA classifiers, making it possible to effectively fine-tune them using any real-world foliage image dataset for improved classification performance. The Foliagen framework is exemplified by generating foliage image datasets for soybean and tomato. Our evaluation results indicate that five SOTA classifiers on generated datasets with nine disease categories achieve accuracy up to 87% for soybean and 86% for tomato under  $\gamma = 5\%$ , and that they all exhibit less than 92% in classifying the real soybean foliage image dataset (with just two disease categories). Foliagen makes it possible to generate crop foliage image datasets to evaluate future disease classifiers objectively, aiming at in-field applications.

## 1 INTRODUCTION

Crops have been indispensable to human civilization since its inception, serving as a fundamental source of food, medicine, clothing, shelter, and oxygen. Extensive pursuits in crop's structure, phyllotaxis phenomenon (Coussement et al., 2018; Koki et al., 1994; Niklas, 1988), life cycle, and disease have been undertaken, aiming at yield improvement to meet growing demands. According to the Food and Agriculture Organization (FAO), crop diseases cost approximately \$220 billion annually in the world (cro, 2021), with soybean alone accounting for a loss up to \$3.9 billion USD in the USA (Bradley et al., 2021). They usually show prominent symptoms, manifesting themselves as changes in the soybean's leaf foliar appearance and/or shape. For example, rust in soybean exhibits small, pale green to yellow spots on the upper surface of leaves (see Figure 1(f)). Since many crop disease categories possibly exist as illustrated in Figures 1 and 2, early disease identification makes it possible to apply proper measures at the onset of diseases for curbing damage they may cause, retaining crop yields as best as possible.

Instead of relying on experienced farmers for disease identification, machine learning (ML) has been adopted (Abbas et al., 2021; Karlekar and Seal, 2020; Pan et al., 2023; Sun et al., 2024a;b; Wu et al., 2023; Yogabalajee et al., 2024) recently to classify soybean and tomato diseased leaf images with success. ML models automate disease classification through training on large amounts of diseased and healthy leaf images. As exemplified in Figures 1 and 2, quality images of individual diseased soybean and tomato leaves exist in public datasets (Bevers et al., 2022; Hughes et al.,

054 2015; Sivm205, 2023) for model training. A state-of-the-art (SOTA) ML model targeting soybean  
 055 disease classification is shown to have an average accuracy above 85% on a non-public dataset of  
 056 individual leaf images gathered from the soybean plantations of the author’s college (Wu et al.,  
 057 2023). Meanwhile, two SOTA ML models for tomato disease classification are demonstrated to  
 058 enjoy high accuracy rates, with one under two public datasets of individual leaf images (given in  
 059 (Gehlot et al., 2023; Hughes et al., 2015)) to exceed 99% (Sun et al., 2024b). Note that those SOTA  
 060 classifiers often resort to specific augmentation strategies; for example, random masking on the  
 061 individual soybean leaf images (Wu et al., 2023) or the Gaussian filter for enhancing and obscuring  
 062 artifacts of individual tomato leaf images (Sun et al., 2024b). Such augmentation strategies can be  
 063 expensive and less effective when applied to images with large numbers of leaves, like crop foliage  
 064 images (see Figure 5 and Figures 6 and 7).

065 Although SOTA ML models (e.g., (Pan et al., 2023; Sun et al., 2024b; Wu et al., 2023; Yoga-  
 066 balajee et al., 2024)) are high classification performers on the existing datasets of individual leaf  
 067 images, they lack practicality, for in-field applications, where sequences of foliage images are usu-  
 068 ally captured over areas of interest by the cameras of unmanned aerial vehicles (UAVs) for disease  
 069 identification. Therefore, accurate automated disease classification on foliage images is essential  
 070 for practical applications. While one early work (Tetila et al., 2017) dealt with a small collection of  
 071 foliage images covering only two diseased categories, it required highly experienced agronomists  
 072 with substantial time and effort to annotate segmented parts of foliage images for accurate clas-  
 073 sification, considered too expensive and impractical to apply for in-field applications where large  
 074 volumes of images are involved. So far, there is just one annotated soybean foliage image dataset  
 075 available to the public, MH-SoyaHealthVision (Shinde and Attar, 2024), and no publicly available  
 076 dataset of tomato foliage images exists, to the best of our knowledge. Unfortunately, the MH-  
 077 SoyaHealthVision dataset fails to include many predominant soybean disease categories (see Figure  
 078 5 and Figures 6 and 7 in Appendix) and is likely to be inadequate to train an effective classifier for  
 079 identifying the diseases at their early stages, since its images were not captured at the disease onset  
 080 and thus often had considerable diseased leaves each.

081 This paper pioneers a framework to generate crop foliage images utilizing available datasets of sin-  
 082 gle leaf images, called Foliagen (short for foliage generation). A generated foliage image dataset can  
 083 be arbitrarily sized, with each of its images having a specified rate of diseased leaves (denoted by  $\gamma$ )  
 084 and the rest being healthy. Such generated datasets are annotated by design, tailored to in-field ap-  
 085 plications for foliage image classification. They are valuable for (1) evaluating the SOTA classifiers  
 086 when applied to practical use and (2) pre-training general SOTA classifiers, making it possible to  
 087 fine-tune them using any real-world foliage image dataset for improved classification performance.  
 088 The Foliagen framework is exemplified by generating foliage image datasets for soybean and tomato,  
 089 using the individual diseased leaf images from ASDID (Bevers et al., 2022), PlantVillage (Hughes  
 090 et al., 2015), and Kaggle (Sivm205, 2023) datasets. It takes as its input (1) the disease category and  
 091 (2) the rate ( $\gamma$ ) of diseased leaves in a foliage image. Each generated foliage image dataset covers  
 092 nine predominant disease categories for soybean and tomato (with samples depicted in Figure 5 and  
 093 Figures 6 and 7 in the Appendix, respectively). Such datasets make it possible to train classifiers for  
 094 early disease identification when generating foliage images at a small  $\gamma$  (say, 5%).

095 Unlike an individual leaf image where background or noise takes up its considerable area, a foliage  
 096 image synthesized by Foliagen is dominated by soybean or tomato leaves, with only a small fraction  
 097 of its area being background (see Figure 5 and Figures 6 and 7 in Appendix). It is found from our  
 098 evaluation results that SOTA models classify nine disease categories less accurately on the generated  
 099 soybean foliage image datasets than on the original individual leaf images, at varying degrees. As  
 100 listed in Table 1 for soybean disease classification, SOTA classifiers are subject to accuracy reduction  
 101 by up to 3% (or 12%) on generated foliage image datasets with  $\gamma = 15\%$  (or 5%), rendering the best  
 102 performer (VGG19 (Simonyan and Zisserman, 2015)) for classifying individual soybean images  
 103 to be less attractive for foliage image classification. Similar performance degradation is observed  
 104 for tomato disease classification, up to 17% (or 22%) reduction in accuracy for Swin Transformer  
 105 (Liu et al., 2021) under generated foliage image datasets with  $\gamma = 15\%$  (or 5%), as shown in Table  
 106 3. The most effective classifier under foliage image datasets is DenseNet121 (Huang et al., 2017),  
 107 instead of VGG19 (Simonyan and Zisserman, 2015) on the datasets of individual tomato leaf images.  
 Hence, Foliagen establishes foliage image datasets useful for candidly assessing known and future  
 classifiers to identify ones that are most effective for in-field applications.

108 In addition, classifiers pre-trained by a generated soybean foliage image dataset with  $\gamma = 15\%$  is  
 109 confirmed to perform equally well (with VGG19 to achieve 93+% accuracy) under the only known  
 110 real-world foliage image dataset (e.g., MH-SoyaHealthVision (Shinde and Attar, 2024)) via em-  
 111 ploying a small fraction of the dataset (say, 10%) to fine-tune the pre-trained classifiers, as the result  
 112 of transfer learning. Classifiers so pre-trained learns abstract features of diseased soybean foliage  
 113 images under various disease categories, making it possible to adapt soundly for classifying the real-  
 114 world foliage images with high accuracy. The overall contributions of this paper are summarized as  
 115 follows:

- 116 • A framework for generating annotated foliage image datasets (Foliagen) is introduced by  
 117 utilizing public datasets of individual crop leaf images. Datasets so generated can be arbi-  
 118 trarily large, properly annotated, and aimed to cover various crop disease categories com-  
 119 mon in the field and to target early disease identification by setting a small  $\gamma$  (say, 5%).
- 120 • Foliagen is exemplified by generating foliage image datasets for soybean and tomato, with  
 121 the generated datasets used for evaluating SOTA classifiers to determine the most effective  
 122 ones for real-world applications.
- 123 • We have demonstrated that generated foliage image datasets can pre-train a general model  
 124 for crop disease classification, so that the pre-trained model can then be fine-tuned by a  
 125 small fraction of any real-world foliage image dataset for high classification accuracy under  
 126 the dataset, as a result of transfer learning.

## 128 2 RELATED WORK

### 131 2.1 PLANT LEAF DATASETS

132 Many plant leaf datasets are available to the public, with some covering a variety of plant species  
 133 each, such as PlantVillage (Hughes et al., 2015) and PlantDoc (Singh et al., 2020), and others being  
 134 plant-specific, including those for soybean and tomato given in (Bevers et al., 2022; Gehlot et al.,  
 135 2023; Hughes et al., 2015; Shinde and Attar, 2024; Sivm205, 2023). Existing plant leaf datasets  
 136 are outlined briefly below, with more details about the PlantVillage dataset (Hughes et al., 2015),  
 137 ASDID (Bevers et al., 2022), a Kaggle dataset (Sivm205, 2023), and the MH-SoyaHealthVision  
 138 dataset (Shinde and Attar, 2024) provided in Section 3.1.

139 **PlantVillage dataset.** PlantVillage (Hughes et al., 2015) contains over 54,300 expertly curated  
 140 healthy and diseased leaf images from various plants, including thirteen major crop species like  
 141 soybean, tomato, etc. Its leaf classification has been attempted by GoogleNet (Szegedy et al., 2015)  
 142 and AlexNet (Krizhevsky et al., 2012) to attain high accuracy.

144 **PlantDoc dataset.** The PlantDoc dataset (Singh et al., 2020) contains 2,598 single-leaf images of 17  
 145 disease categories across 13 plant species, including tomato and soybean. With its images gathered  
 146 in a controlled laboratory environment, this dataset has limited applicability in real-world scenarios.

147 **ASDID.** Auburn Soybean Diseased Image Dataset (ASDID) (Bevers et al., 2022) provides high-  
 148 quality individual leaf images of the soybean plant, covering 9 disease categories, namely, bacterial  
 149 blight, cercospora leaf blight, downy mildew, frogeye leaf spot, soybean rust, target spot, and potas-  
 150 sium deficiency. The dataset was captured primarily at the EV Smith Agricultural Research Station  
 151 in Tallahassee, Alabama, and added with 80 images per disease category from the publicly available  
 152 Image Database of Plant Disease Symptoms (PDDB) (Barbedo et al., 2016). Several ML-based  
 153 classifiers (He et al., 2016; Huang et al., 2017; Simonyan and Zisserman, 2015) were employed to  
 154 evaluate the dataset, with DenseNet201 (Huang et al., 2017) achieving the highest performance.

155 **Kaggle dataset.** Soybean Diseased Leaf Dataset contains individual leaf images from Kaggle  
 156 (Sivm205, 2023), embracing 10 disease categories and having an artificially generated complex  
 157 background added to each image. Among the 10 diseases, only mosaic virus and sudden death  
 158 syndrome are considered.

159 **FieldPlant dataset.** FieldPlant (Moupojou et al., 2023) is a dataset of individual crop leaf images  
 160 annotated by pathologists, containing 8,629 images across 27 disease categories for three crops,  
 161 including tomato. It aims at practical crop disease classification with every leaf image involving a  
 complex background.

162 **Tomato-Village dataset.** Compensating for the negative effects due to the laboratory-controlled environment setup for gathering PlantVillage’s leaf images, the Tomato-Village dataset (Gehlot et al., 163 2023) contains real-world images, which belong to three groups, respectively for (1) multi-class 164 tomato disease classification, (2) multi-label tomato disease classification, and (3) object detection- 165 based tomato disease detection. This dataset covers seven disease categories, namely, early blight, 166 late blight, leaf miner, magnesium deficiency, nitrogen deficiency, potassium deficiency, and spotted 167 wilt virus, for multi-class classification applications.

168 **MH-SoyaHealthVision dataset.** As far as we know, MH-SoyaHealthVision (Shinde and Attar, 169 2024) is the only public and well-annotated dataset of diseased soybean foliage images. The dataset 170 provides both ground-level leaf images and foliage leaf images, collected using a UAV, from the 171 soybean fields of Maharashtra, India. It comprises a total of 5,680 high-resolution images grouped 172 into (1) single leaf images of 4 diseases categories (i.e., frogeye, mosaic virus, septoria brown spot, 173 and rust), two types of pest attacks, and healthy leaves and (2) UAV-captured soybean foliage images, 174 which belong to two disease categories of mosaic virus and rust, plus the healthy category.

175 All the above datasets were reviewed and carefully examined for possible use by our Foliagen framework; however, only the PlantVillage, ASDID, and the Kaggle datasets were selected as single-leaf 176 image sources due to their large numbers of well-annotated images, with high fidelity and clarity.

177

## 178 2.2 GENERATION METHODS

179 Synthetic dataset generation has been widely adopted in the field of computer vision, especially in 180 areas such as disease detection, object detection, and segmentation, where data collection is very 181 costly and time-consuming. Various methods have been experimented with in previous research 182 to augment image data, including simple copy & paste, graphical method (Bradley et al., 2013), 183 and machine learning techniques. Simple copy & paste has been utilized to augment data (Guo, 184 2024; Higuchi et al., 2023), and found to be effective for object detection (Dwibedi et al., 2017), 185 image classification (Mesnage et al., 2025), and instance segmentation (Ghiasi et al., 2021; Remez 186 et al., 2018; Shen and Li, 2023). (Dwibedi et al., 2017) introduced the concept of cut and paste to 187 augment image data for instance detection, demonstrated to yield marked improvements under the 188 LVIS benchmark (Ghiasi et al., 2021) and improved training performance for ultrasound instance 189 segmentation (Shen and Li, 2023).

190 Deep learning (DL) methods were also implemented to augment leaf data, such as LeafNST (Khare 191 et al., 2024), NeuraLeaf (Yang et al., 2025), LeafGAN (Cap et al., 2020), and others (Benfenati 192 et al., 2022; Ward et al., 2018). Particularly, (Benfenati et al., 2022) adopted a Residual Variational 193 Autoencoder for leaf generation and a generative adversarial network, Pix2pix, for color translation 194 on generated leaf images. Similarly, LeafNST Khare et al. (2024) transfers the symptoms of diseased 195 leaves into healthy leaves to enlarge the diseased leaf count. While these DL models are proven to 196 be effective for data augmentation, they are limited to single leaf images, inevitably constraining 197 their usage in the real world.

198

## 199 2.3 CROP LEAF DISEASE CLASSIFICATION MODELS

200

201 Automated disease classification studies have been conducted lately based on the aforementioned 202 publicly available datasets, plus certain privately collected datasets, to exhibit impressive classifi- 203 cation outcomes (Abbas et al., 2021; Bouni et al., 2024; Karlekar and Seal, 2020; Pan et al., 2023; 204 Sun et al., 2024a;b; Wu et al., 2023; Yogabalajee et al., 2024; Yu et al., 2022). Bevers *et al.* (Bev- 205 ers et al., 2022) in Auburn, AL collected a high-quality single leaf imagery dataset and employed 206 standard CNN-based models, such as VGG19, DenseNet201, and ResNet50, etc., to classify their 207 collected dataset, achieving high accuracy. Enhanced DenseNet121 (Yogabalajee et al., 2024) re- 208 lied on transfer learning to tackle the intricate challenges of classifying individual soybean leaf 209 images. Using a conditional generative adversarial network (C-GAN) to generate synthetic 210 individual tomato diseased leaves, previous work (Abbas et al., 2021) achieved very high performance 211 employing DenseNet121 (Huang et al., 2017) as its classification model. Merging classical feature 212 engineering with modern machine learning techniques, Bouni *et al.* (Bouni et al., 2024) recently 213 have employed a CNN pre-trained on ImageNet (Deng et al., 2009) under mutual information-based 214 feature fusion to get a high performer for tomato disease classification.

216 While CNN-based models can capture the prominent features of images, incorporating an attention  
 217 mechanism into the models enables them to emphasize the region that contributes most to performance  
 218 improvement. Previous studies incorporating attention mechanisms (Hu et al., 2018; Liu  
 219 et al., 2021; Sun et al., 2024a;b; Wang et al., 2020; Woo et al., 2018; Wu et al., 2023) have been  
 220 proven effective for computer vision tasks, such as image segmentation, image classification, and  
 221 object detection targeting leaf disease classification, where leaf colors and shapes are key features of  
 222 interest (Pan et al., 2023; Wu et al., 2023). Swin Transformer (Liu et al., 2021) introduces a hierar-  
 223 chical segmentation along with the vision transformer to implement shifted windows, which capture  
 224 main features across different segmentation regions of an image. Meanwhile, CBAM-ConvNeXt  
 225 (Wu et al., 2023) employs both channel attention and spatial attention plus ConvNeXt (Liu et al.,  
 226 2022), to classify the individual soybean leaf images, which are not publicly available yet. While  
 227 exhibiting impressive feats, all known studies (but (Tetila et al., 2017)) aim only at classifying high-  
 228 resolution images of individual crop leaves, as illustrated in Figures 1 and 2.  
 229

### 230 3 METHODOLOGY

231 The Foliagen framework generates diseased foliage images out of available single-leaf diseased  
 232 images for the classification of diseased foliage images for (1) objectively evaluating known and  
 233 future crop disease classifiers when deployed for in-field applications and (2) pre-training general  
 234 crop disease classifiers, making them tailored for specific fields with high classification performance  
 235 after fine-tuned by a small number of annotated foliage images gathered in those fields, as the result  
 236 of transfer learning. It is exemplified by generating foliage images of soybean and tomato, leveraging  
 237 three publicly available individual-leaf image datasets, ASDID Bevers et al. (2022), a Kaggle dataset  
 238 Sivm205 (2023), and the PlantVillage dataset (Hughes et al., 2015), which are detailed in Section  
 239 3.1. Single soybean leaf images are preprocessed (as described in Section 3.1) before being utilized  
 240 by Foliagen to generate diverse sets of foliage images for evaluating known classifiers objectively.  
 241 Such a single image manipulation methods has been proven to be effective for image segmentation  
 242 and object detection data augmentation (Dwibedi et al., 2017; Ghiasi et al., 2021; Remez et al.,  
 243 2018). In addition, known classifiers after being pre-trained by generated foliage images that cover  
 244 9 disease categories are fine-tuned via 10% of images from the real-world soybean foliage image  
 245 dataset, MH-SoyaHealthVision Shinde and Attar (2024), and are found to classify the remaining  
 246 80% MH-SoyaHealthVision images with improved performance.  
 247

#### 248 3.1 DATA COLLECTION

249 **Soybean.** A total of 10,722 high-resolution single leaf images covering 7 disease categories from  
 250 ASDID Bevers et al. (2022) and 132 images (with 22 for Mosaic Virus and 110 for sudden Death  
 251 Syndrome) from a Kaggle dataset (Sivm205, 2023) were chosen for foliage image generation. Im-  
 252 ages of those nine disease categories (as depicted in Figure 1) feature diverse and complex natu-  
 253 ral/artificial backgrounds, which are undesirable when generating foliage images. Therefore, we  
 254 pre-process the images to remove their undesired backgrounds (i.e., to make them transparent) us-  
 255 ing an open-sourced and AI-enabled background remover, rembg (Gatis, 2021), as shown in the first  
 256 stage of Overall Foliagen depicted in Figure 3. Freely available soybean field soil images are then  
 257 included in generated foliage images as their backgrounds, to emulate the natural habitat of soybean  
 258 plants as best as possible.  
 259

260 The only publicly available and properly annotated dataset of diseased foliage images, MH-  
 261 SoyaHealthVision (Shinde and Attar, 2024), comprises two disease categories: soybean rust and  
 262 mosaic virus. The original images have a very high resolution of  $3840 \times 2160$  and the dataset is  
 263 imbalanced, with rust images outnumbering healthy images by a factor of four, leading to biased  
 264 predictions favoring the majority class and consequently reducing the model’s generalizability. To  
 265 address these issues, we crop the high-resolution foliage images into ones with a lower resolution to  
 266 ensure a more balanced data distribution and to obtain a total of 3210 images, comprising 1084 rust  
 267 images, 1027 healthy images, and 1099 mosaic virus images, respectively.  
 268

269 **Tomato.** The single-leaf diseased images of tomato are from the PlantVillage dataset (Hughes et al.,  
 270 2015), with 9 primary tomato disease categories, and they are taken in a laboratory environment and  
 271 with the dimension of  $256 \times 256$ , as shown in Figure 2.

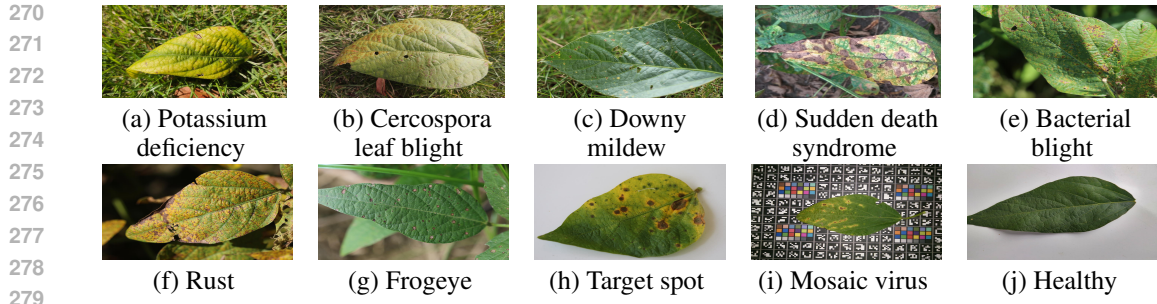


Figure 1: Soybean single-leaf images of 9 diseases, labeled by (a) to (i).

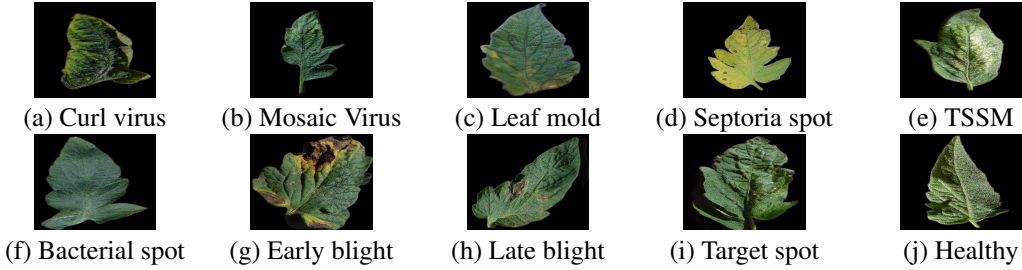


Figure 2: Tomato single leaf images of 9 diseases, labeled by (a) to (i).

### 3.2 FOLIAGEN FRAMEWORK

Foliagen takes pre-processed individual leaf images as input to generate foliage images with a customizable rate of diseased leaves. After preprocessing single leaf images for background removal via rembg (Gatis, 2021), it then involves 3 levels of generation, Leaf Level, Plant Level, and Foliage Level, as depicted in Figure 3. Each level incorporates plant-specific information such as disease categories, target disease rate, and inherent leaf structural characteristics, as denoted by ‘Configuration File’ in Figure 3. The structure of the configuration file used to provide this information is detailed in Appendix A.6.

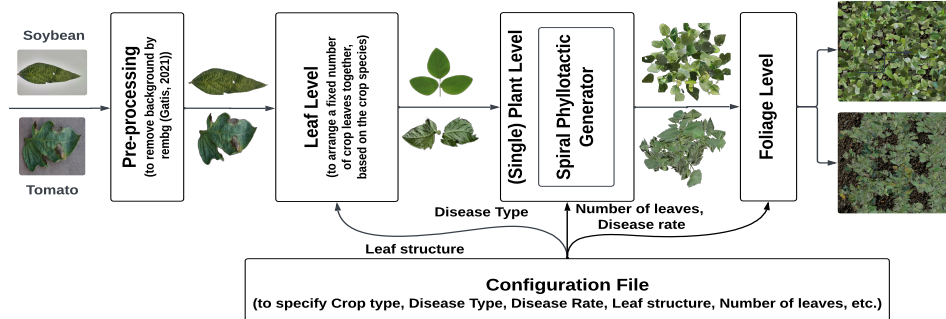


Figure 3: Overall Foliagen.

**Leaf Level.** Soybean leaves arrange themselves into 3 leaflets in each petiole, with a slightly bigger central leaflet and two lateral leaflets on the two side of the central leaflet, as illustrated in Figure 3. On the other hand, tomato leaves arrange themselves around a central axis, called the rachis. In practice, crop leaflets may or may not be diseased. Hence, a random number of healthy leaflets are included in each foliage image, governed by the disease rate  $\gamma$ .

**Plant Level.** The number of leaves in an adult crop differs largely, based on the crop. An adult soybean plant might contain 30-40 trifoliates, while an adult tomato plant may have 20-40 leaves, assuming the determinate variety of tomato crop. Both crops exhibit spiral phyllotaxis (Koki et al., 1994; Niklas, 1988), in which leaves are arranged in a spiral arrangement that makes the golden angle, i.e,  $137.5^\circ$ , to maximize sunlight exposure and minimize leaf overlap. Most of the leaves in

324 a crop are healthy in the early stages of a disease, so foliagen takes a small disease rate  $\gamma$  (e.g., 5%  
 325 or 15%). A spiral phyllotactic coordinates generator is the vital part of this Plant level, following  
 326 the formulae given below to determine the coordinates and the angles of leaves to maintain spiral  
 327 phyllotaxis (Niklas, 1988).

- 329 • Center:  $(x_0, y_0)$ , Golden angle:  $\theta_g^{rad} = 137.5^\circ \times \frac{\pi}{180} = 1.57$ , Scaling factor:  $s = 35$
- 330 • Number of trifoliates:  $N = X \sim \mathcal{U}\{30, 31, \dots, 40\}$

331 For each trifoliate index  $n \in \{1, 2, \dots, N\}$ :

$$332 \text{Angular displacement: } \theta_n = n \cdot \theta_g^{rad} \quad \text{Radial distance: } r_n = s \cdot \sqrt{n}$$

$$333 \text{Cartesian coordinates: } \begin{cases} x_n = x_0 + r_n \cos(\theta_n) \\ y_n = y_0 + r_n \sin(\theta_n) \end{cases}$$

336 The final discrete leaf positions are expressed by:

$$338 coords = \{(\lfloor x_n \rfloor, \lfloor y_n \rfloor) \mid n = 1, 2, \dots, N\},$$

339 where  $\lfloor \cdot \rfloor$  denotes the integer truncation.

340 As a tomato plant has branches, with a pair of leaves attached at a similar stem height and arranged  
 341 in opposite directions, a sub-layer, called the branch layer, is added to create branches, each with  
 342 3-9 leaves. Such an emulated branch is then attached to the main stem in spiral phyllotactical order.

343 **Foliage Level.** Foliage images usually consist of multiple rows of crops planted in a farm field.  
 344 Observation from real-world images taken using UAVs Shinde and Attar (2024) reveals that the  
 345 major area of an image is covered by leaves, with only a small area being field soil (Freepik, 2025).  
 346 As a result, Foliagen generates images with three rows of crops in each image to emulate their  
 347 natural appearance. Samples of generated foliage images are illustrated in Figure 5 and Figures 6  
 348 and 7 in Appendix A.1.

### 350 3.3 DISEASE DISTRIBUTION

351 The distribution of disease in plant leaves is influenced by multiple interacting factors, including  
 352 insect vectors, wind-mediated spore dispersal, plantation age, and environmental conditions, such  
 353 as humidity, rainfall, and temperature. Although the spatial pattern of disease may vary consider-  
 354 ably depending on these influences, a consistent phenomenon is that infections generally begin  
 355 as localized hotspots on leaves or within a small plant patch and subsequently spread outward to  
 356 one (or multiple) neighboring patch(es), ultimately forming a larger area of diseased foliage (Chen  
 357 et al., 2025; Tao et al., 2021; Yang et al., 1991). This diseased leaf distribution is confirmed by  
 358 us through examining the real-world foliage images of various disease categories in the available  
 359 MH-SoyaHealthVision dataset (Shinde and Attar, 2024) (see Figure 4(c)), leading us to devise a  
 360 three-level disease distribution pattern, as explained next.

361 **Region Level.** The whole image is divided into a  $\alpha \times \beta$  grid with a total of  $\alpha \times \beta$  regions. e.g.,  $4 \times 3$   
 362 = 12 regions. Most regions are disease-free when the disease rate ( $\gamma$ ) is small, say  $\leq 20\%$  and every  
 363 diseased region is provided with a disease rate, so that all  $\alpha \times \beta$  regions have the aggregate disease  
 364 rate of  $\gamma$ . The diseased leaves in a diseased region are distributed normally across the region.

365 **Patch Level.** A patch refers to a collection of adjacent regions with one hotspot and its neighboring  
 366 regions. Based on the disease rate, the number of diseased patches in a single foliage image varies  
 367 from 1 to 2 under our disease rate of interest to be less than 20% for early disease identification.  
 368 Naturally, a higher disease rate is expected to yield more disease patches in a patch. The distribution  
 369 of the number of hotspots among the foliage images follows a skewed graph. Figure 4(b) shows the  
 370 distribution of two hotspots for the mean disease rate of 15%, where the number of hotspot disease  
 371 patches per image being 1 (or 2) equals 1,721 (or 6,279) out of 8,000 total generated foliage images.

372 **Dataset Level.** The disease rate of the foliage images is normally distributed with the standard  
 373 deviation ( $\sigma$ ) of 1.5 and the variable mean ( $\mu = \gamma$ ) of 15% (or 5%). Figure 4(a) depicts the disease  
 374 rate distribution for  $\gamma = 15\%$ , where the disease rate varies from 10% to 20%. For  $\gamma = 5\%$ , the  
 375 disease rate ranges from 1% to 9%, with a similar normal distribution as illustrated in Figure 4(a).

376 **Crop Level Customization.** Foliagen is a common framework, aiming to generate a foliage imagery  
 377 dataset for various crops out of those crops' single leaf images. Given crops differ among one

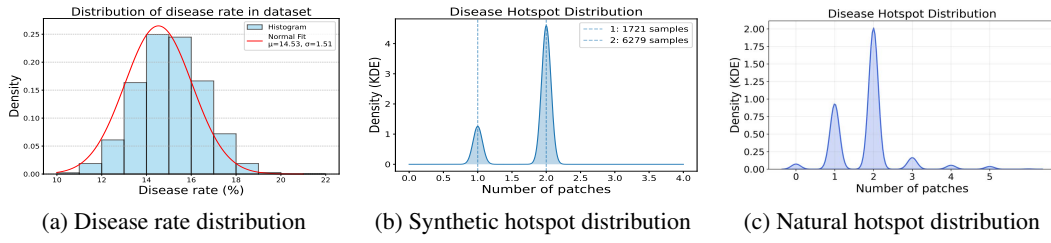


Figure 4: Disease distributions, (a) and (b) across synthetic diseased soybean foliage datasets ( $\gamma = 15\%$ ), and (c) for the natural foliage dataset (MH-SoyaHealthVision).

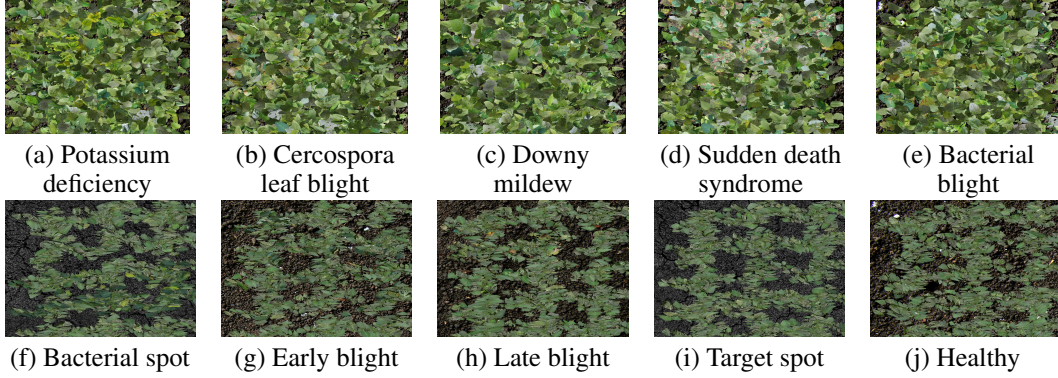


Figure 5: Generated soybean foliage images (a)-(e) and tomato foliage images (f)-(j), for  $\gamma = 15\%$ . (All generated foliage image categories for soybean and tomato are shown respectively in Figures 6 and 7 in Appendix A.1.)

another in many factors, such as the leaf shapes, the leaf arrangements, phyllotaxis, number of leaves in single branch, numbers of leaves in single branches, etc., Foliagen is provisioned with a configuration file as its input to account for the crops’ variability, with the file listing such crop-specific customization parameters as the disease rate, the size of individual leaf, the size of individual plant, the foliage size, disease categories, etc., to properly emulate crops’ natural structures.

## 4 EVALUATION AND RESULT DISCUSSION

Extensive experiments to evaluate the performance of SOTA crop disease classifiers on generated foliage images are conducted on two workstations, with one housing 2 NVIDIA GeForce RTX 3090 GPUs (each with 24 GB of GDDR6X VRAM) and another housing 2 NVIDIA RTX 6000 Ada GPUs (each with 48 GB of GDDR6X VRAM). The foliage image datasets of soybean and tomato for  $\gamma = 5\%$  and  $15\%$  (to emulate the early stage of disease) have been generated for evaluation, with the sensitivity results of classifiers to a wide range of disease rates provided in Appendix A.4. Each generated foliage image dataset contains about 800 images for every disease category, plus a similar number of healthy foliage images. The Adam optimizer was used for model training, since it is known to converge faster with better performance by dynamically adjusting the learning rate for each parameter based on the first and second moments of gradients. Each model was trained for a maximum of 100 epochs, with an early stopping mechanism (with patience of 5 epochs) to avoid local minima. The batch size was set to 4, restricted by the GPU memory limitation, and the learning rate was initialized to 0.000001.

### 4.1 EVALUATION ON GENERATED SOYBEAN FOLIAGE IMAGE DATASETS

Various generated soybean foliage image datasets under different  $\gamma$  (the rate of diseased leaves in each foliage image) values have been produced by Foliagen to objectively evaluate the SOTA disease classification models of VGG19 (Simonyan and Zisserman, 2015), ResNet50 (He et al., 2016), DenseNet121 (Huang et al., 2017), Swin Transformer (Liu et al., 2021), and CBAM-ConvNeXt (Wu et al., 2023) under exactly the same set of foliage images without any classifier-specific data pre-processing or manipulation. Each produced foliage image dataset covers all crop disease categories

that exist in the original datasets of individual leaf images, with a small  $\gamma$  (say, 5%) to indicate an early disease stage. The evaluation results shed light on choosing the best classifier among those SOTA models for real-world soybean applications, where disease identification is based on in-field images captured by cameras mounted on UAVs. The evaluation metric outcomes under a synthetic dataset with a larger  $\gamma$  are expected to be higher because more diseased leaves exist in each foliage image, making disease classification easier. The comparative performance evaluation results are obtained for  $\gamma$  ranging from 5% to 15% and beyond, and they are found to follow similar trends. For simplicity, only the results for  $\gamma = 5\%$  to 15% are listed in Table 1. It is evident from the table that DenseNet121 prevails for both  $\gamma$  values, in terms of all the metrics.

Table 1: Comparative performance evaluation results (in %) under generated soybean foliage image dataset with  $\gamma = 15\%$  (or 5%)

Models	Accuracy	F1-score	Precision	Recall
VGG19 (Simonyan and Zisserman, 2015)	76.26 (65.45)	77.17 (65.67)	78.11 (66.19)	76.26 (65.15)
ResNet50 (He et al., 2016)	85.31 (81.91)	85.40 (83.58)	85.69 (85.37)	85.11 (81.87)
DenseNet121 (Huang et al., 2017)	<b>94.47</b> ( <b>87.56</b> )	<b>95.45</b> ( <b>90.81</b> )	<b>96.45</b> ( <b>94.45</b> )	<b>94.48</b> ( <b>87.44</b> )
Swin Transformer (Liu et al., 2021)	72.36 (65.38)	72.99 (64.50)	72.37 (63.62)	72.68 (65.41)
CBAM-ConvNeXt (Wu et al., 2023)	77.76 (66.33)	79.73 (69.59)	81.84 (73.15)	77.72 (66.36)

## 4.2 EVALUATION ON REAL SOYBEAN FOLIAGE IMAGE DATASET

**Baseline.** The MH-SoyaHealthVision dataset (Shinde and Attar, 2024) was split into 80% for training, 10% for validation, and 10% for evaluation, enabling an objective evaluation of the same five SOTA classifiers under exactly the same set of real-world foliage images without any data pre-processing or manipulation. From the comparative performance results summarized under Baseline of Table 2, it is found that Swin Transformer achieves the highest performance, with accuracy exceeding 91% across all four metrics, whereas other models have the accuracy values ranging from 85<sup>+</sup>% to 89<sup>-</sup>%. The baseline results indicate that Swin Transformer is the top performer for real-world applications.

**Transfer Learning.** Generated foliage image datasets can pre-train crop disease classification models to get powerful disease classifiers suitable for general applications. After those five SOTA models are pre-trained by our generated foliage images to cover nine categories of predominant soybean diseases, they are expected to serve as general classifiers for effectively identifying any real-world dataset of soybean foliage images at hand by fine-tuning them using a small fraction of foliage images in the dataset, due to transfer learning. When classifiers are pre-trained by a generated foliage image dataset with a small  $\gamma$  (say, 5%), they are geared for identifying soybean diseases at an early stage, especially useful for real-world field applications. To this end, the trained models are evaluated under the real-world MH-SoyaHealthVision dataset (Shinde and Attar, 2024), after being fine-tuned via 5% images in the dataset, with the evaluation results listed under Pre-trained in Table 2. Note that the results are obtained when 10% and 85% dataset images are for validation and evaluation, respectively, after 5% images are employed for fine-tuning. Comparing the obtained evaluation results shown in Table 2, we find that the trained models with fine-tuning elevate performance metric values noticeably, to exceed 92% in accuracy for DenseNet121, ResNet50, CBAM-ConvNeXt, and Swin Transformer under  $\gamma = 15\%$ . The performance results of pre-trained models are worse under  $\gamma = 5\%$  than under  $\gamma = 15\%$ , as expected, since the former aimed to detect diseases in an early stage, known to be harder but more useful. They also signify that Swin Transformer is the most desirable for in-field applications, when aiming at early disease detection (under  $\gamma = 5\%$ ).

Table 2: Comparative performance evaluation results (in %) under MH-SoyaHealthVision

Models	Baseline				Pre-trained with $\gamma = 15\%$ (or 5%)			
	Accuracy	F1-score	Precision	Recall	Accuracy	F1-score	Precision	Recall
VGG19	85.38	86.6	87.98	85.38	88.00 (84.03)	88.22 (84.06)	88.41 (84.08)	88.03 (84.03)
ResNet50	88.31	89.69	91.11	88.31	<b>95.83</b> (90.61)	<b>95.91</b> (90.86)	<b>95.98</b> (91.12)	<b>95.84</b> (90.60)
DenseNet121	87.5	87.95	88.37	87.5	94.40 ( <b>94.47</b> )	94.48 ( <b>94.19</b> )	94.55 ( <b>94.29</b> )	94.40 ( <b>94.08</b> )
Swin Transformer	<b>91.48</b>	<b>91.47</b>	<b>91.46</b>	<b>91.48</b>	92.32 (87.57)	91.33 (88.52)	90.39 (89.51)	92.29 (87.56)
CBAM-ConvNeXt	88.82	87.06	85.39	88.83	95.38 (86.76)	95.37 (88.06)	95.36 (89.42)	95.38 (86.74)

486 4.3 TOMATO  
487

488 Foliagen synthesizes various disease datasets of tomato foliage images based on the PlantVillage  
489 dataset (Hughes et al., 2015) (publicly available datasets of single leaf images with 9 primary tomato  
490 disease categories), under a range of  $\gamma$  for evaluating the SOTA classifiers. The evaluation metric  
491 outcomes under a generated dataset with a larger  $\gamma$  are expected to be higher because more diseased  
492 leaves exist in each foliage image, making disease classification easier. Given that the comparative  
493 evaluation results are obtained for  $\gamma$  ranging from 5% to 15% and beyond follow similar trends,  
494 Table 3 lists only the results for  $\gamma = 5\%$  and 15%. As evident from the table, the considered models  
495 all perform better under 15% than under 5% with respect to the four performance metrics, under-  
496 scoring the fact that they tend to struggle in early disease detection (under  $\gamma = 5\%$ ), especially for  
497 VGG19, ResNet50, and Swin Transformer. The evaluation results imply that DenseNet121 out-  
498 performs the rest consistently, making it the most desirable classifier for in-field applications for  
499 identifying tomato diseases according to foliage images captured in the field by UAVs.  
500

501 Table 3: Comparative performance evaluation results (in %) under generated tomato foliage image  
500 dataset with  $\gamma = 15\%$  (or 5%)

502 Models	503 Accuracy	504 F1-score	505 Precision	506 Recall
502 VGG19 (Simonyan and Zisserman, 2015)	503 87.66 (80.53)	504 87.71 (81.01)	505 87.64 (81.51)	506 87.78 (80.50)
502 ResNet50 (He et al., 2016)	503 92.22 (78.84)	504 92.44 (81.39)	505 92.65 (84.11)	506 92.23 (78.83)
502 DenseNet121 (Huang et al., 2017)	503 <b>96.38</b> ( <b>86.93</b> )	504 <b>97.34</b> ( <b>89.47</b> )	505 <b>97.69</b> ( <b>92.16</b> )	506 <b>96.99</b> ( <b>86.93</b> )
502 Swin Transformer (Liu et al., 2021)	503 79.80 (66.53)	504 79.36 (66.71)	505 78.84 (66.81)	506 79.88 (66.60)
502 CBAM-ConvNeXt (Wu et al., 2023)	503 81.91 (64.85)	504 81.68 (65.56)	505 82.96 (66.24)	506 81.96 (64.89)

507 5 CONCLUSION  
508

509 This article introduces a framework (called Foliagen) to generate rich and arbitrarily-sized datasets  
510 of crop foliage images to cover all disease categories that exist in publicly available datasets of in-  
511 dividual leaf images, with a given rate of diseased leaves ( $\gamma$ ) in each foliage image generated to  
512 emulate the real foliage images captured in farm fields when their crop diseases are at the stage  
513 corresponding to  $\gamma$ . The generated foliage datasets are employed to better and objectively eval-  
514 uate state-of-the-art leaf disease classifiers without invoking classifier-specific data pre-processing or  
515 manipulation. The evaluation results make it possible to choose the most effective crop classifier  
516 among SOTA ones for in-field applications with UAV-captured images (rather than individual leaf  
517 images) for disease identification. Being a generated foliage dataset, its primary limitation lies in  
518 the lack of naturalness and limited real-world applicability; however, the strong performance of crop  
519 disease classifiers pre-trained on it suggests its potential viability for broader applications. With an  
520 available in-field foliage dataset, the pre-trained models can be fine-tuned using a small fraction of  
521 the dataset images to yield effective disease classifiers targeting the field where the foliage dataset  
522 is gathered. While Foliagen is exemplified for classifying soybean and tomato diseases via SOTA  
523 models in this paper, it is readily useful for other crops and for objectively evaluating future disease  
524 classifiers aiming at in-field applications.

525 REFERENCES  
526

527 Pathogens, precipitation and produce prices. *Nature Climate Change*, 11(8):635–635, 2021.

528 Amreen Abbas, Sweta Jain, Mahesh Gour, and Swetha Vankudothu. Tomato plant disease detection  
529 using transfer learning with c-gan synthetic images. *Computers and Electronics in Agriculture*,  
530 187:106279, 2021.

531 Jayme Garcia Arnal Barbedo, Luciano Vieira Koenigkan, and Thiago Teixeira Santos. Identifying  
532 multiple plant diseases using digital image processing. *Biosystems Engineering*, 147:104–116,  
533 2016. ISSN 1537-5110. doi: <https://doi.org/10.1016/j.biosystemseng.2016.03.012>.

534 Alessandro Benfenati, Davide Bolzi, Paola Causin, and Roberto Oberti. A deep learning generative  
535 model approach for image synthesis of plant leaves. *Plos one*, 17(11):e0276972, 2022.

536 Noah Bevers, Edward J Sikora, and Nate B Hardy. Soybean disease identification using original field  
537 images and transfer learning with convolutional neural networks. *Computers and Electronics in  
538 Agriculture*, 203:107449, 2022.

540 Mohamed Bouini, Badr Hssina, Khadija Douzi, and Samira Douzi. Synergistic use of handcrafted  
 541 and deep learning features for tomato leaf disease classification. *Scientific Reports*, 14(1):26822,  
 542 2024.

543 Carl A. Bradley, Tom W. Allen, Adam J. Sisson, Gary C. Bergstrom, Kaitlyn M. Bissonnette, Jason  
 544 Bond, Emmanuel Byamukama, Martin I. Chilvers, Alyssa A. Collins, John P. Damicone, Anne  
 545 E. Dorrance, Nicholas S. Dufault, Paul D. Esker, Travis R. Faske, Nicole M. Fiorellino, Loren  
 546 J. Giesler, Glen L. Hartman, Clayton A. Hollier, Tom Isakeit, Tamra A. Jackson-Ziems, Douglas  
 547 J. Jardine, Heather M. Kelly, Robert C. Kemerait, Nathan M. Kleczewski, Alyssa M. Koehler,  
 548 Robert J. Kratochvil, James E. Kurle, Dean K. Malvick, Samuel G. Markell, Febina M. Mathew,  
 549 Hillary L. Mehl, Kelsey M. Mehl, Daren S. Mueller, John D. Mueller, Berlin D. Nelson, Charles  
 550 Overstreet, G. Boyd Padgett, Paul P. Price, Edward J. Sikora, Ian Small, Damon L. Smith, Terry  
 551 N. Spurlock, Connie A. Tande, Darcy E.P. Telenko, Albert U. Tenuta, Lindsey D. Thiessen, Fred  
 552 Warner, William J. Wiebold, and Kiersten A. Wise. Soybean yield loss estimates due to diseases in  
 553 the united states and ontario, canada, from 2015 to 2019. *Plant Health Progress*, 22(4):483–495,  
 554 2021.

555 Derek Bradley, Derek Nowrouzezahrai, and Paul Beardsley. Image-based reconstruction and syn-  
 556 thesis of dense foliage. *ACM Transactions on Graphics (TOG)*, 32(4):74:1–74:10, 2013.

557 Quan Huu Cap, Hiroyuki Uga, Satoshi Kagiwada, and Hitoshi Iyatomi. Leafgan: An effective data  
 558 augmentation method for practical plant disease diagnosis. *arXiv preprint arXiv:2002.10100*,  
 559 2020.

560 Chen Chen, Harald Keunecke, Enzo Neu, Friedrich J Kopisch-Obuch, Bruce A McDonald, and  
 561 Jessica Stapley. Molecular epidemiology of cercospora leaf spot on resistant and susceptible  
 562 sugar beet hybrids. *Plant Pathology*, 74(1):69–83, 2025.

563 Jonas Coussement, Michael Henke, Peter Lootens, Isabel Roldán-Ruiz, Kathy Steppe, and Tom  
 564 De Swaef. Modelling leaf spectral properties in a soybean functional-structural plant model by  
 565 integrating the prospect radiative transfer model. *Annals of Botany*, 122(4):669–676, 2018.

566 Jia Deng, Wei Dong, Richard Socher, Li-Jia Li, Kai Li, and Li Fei-Fei. Imagenet: A large-scale  
 567 hierarchical image database. In *Proceedings of IEEE Conference on Computer Vision and Pattern  
 568 Recognition (CVPR)*, pages 248–255. IEEE, 2009. doi: 10.1109/CVPR.2009.5206848.

569 Debidatta Dwibedi, Ishan Misra, and Martial Hebert. Cut, paste and learn: Surprisingly easy syn-  
 570 thesis for instance detection. In *Proceedings of the IEEE International Conference on Computer  
 571 Vision (ICCV)*, pages 1301–1310, 2017.

572 Freepik. Freepik: Graphic resources for everyone. <https://www.freepik.com/>, 2025.

573 Daniel Gatis. rembg: Remove image background. <https://github.com/danielgatis/rembg>, 2021. Accessed: 2025-05-08.

574 Mamta Gehlot, Rakesh Kumar Saxena, and Geeta Chhabra Gandhi. Tomato-village: a dataset for  
 575 end-to-end tomato disease detection in a real-world environment. *Multimedia Systems*, 29(6):  
 576 3305–3328, 2023.

577 Golnaz Ghiasi, Yin Cui, Aravind Srinivas, Rui Qian, Tsung-Yi Lin, Ekin D Cubuk, Quoc V Le, and  
 578 Barret Zoph. Simple copy-paste is a strong data augmentation method for instance segmen-  
 579 tation. In *Proceedings of the IEEE/CVF Conference on Computer Vision and Pattern Recognition  
 580 (CVPR)*, pages 2918–2928, 2021.

581 Quishi Guo. Enrich the content of the image using context-aware copy paste. *arXiv preprint  
 582 arXiv:2407.08151*, 2024.

583 Kaiming He, Xiangyu Zhang, Shaoqing Ren, and Jian Sun. Deep residual learning for image recog-  
 584 nition. In *Proceedings of the IEEE/CVF conference on computer vision and pattern recognition  
 585 (CVPR)*, pages 770–778, 2016.

586 Keita Higuchi, Taiyo Mizuhashi, Fabrice Matulic, and Takeo Igarashi. Interactive generation of  
 587 image variations for copy-paste data augmentation. In *Proceedings of the Extended Abstracts of  
 588 the 2023 CHI Conference on Human Factors in Computing Systems*, pages 1–7, 2023.

594 Jie Hu, Li Shen, and Gang Sun. Squeeze-and-excitation networks. In *Proceedings of the IEEE/CVF*  
 595 *Conference on Computer Vision and Pattern Recognition (CVPR)*, pages 7132–7141, 2018.  
 596

597 Gao Huang, Zhuang Liu, Laurens Van Der Maaten, and Kilian Q Weinberger. Densely connected  
 598 convolutional networks. In *Proceedings of the IEEE/CVF Conference on Computer Vision and*  
 599 *Pattern Recognition (CVPR)*, pages 4700–4708, 2017.

600 David Hughes, Marcel Salathé, et al. An open access repository of images on plant health to enable  
 601 the development of mobile disease diagnostics. *arXiv preprint arXiv:1511.08060*, 2015.  
 602

603 Aditya Karlekar and Ayan Seal. SoyNet: Soybean leaf diseases classification. *Computers and*  
 604 *Electronics in Agriculture*, 172:105342, 2020.

605 Omkar Khare, Sachin Mane, Harish Kulkarni, et al. Leafnst: an improved data augmentation method  
 606 for classification of plant disease using object-based neural style transfer. *Discov Artif Intell*, 4:  
 607 50, 2024.

608 Kanahama Koki, Iwabuchi Kazunori, and Minoru Suda. Phyllotaxis on the main shoot of wild  
 609 tomato plants calculated by the parastichy system. *Tohoku Journal of Agricultural Research*, 44:  
 610 1–4, 1994.  
 611

612 Alex Krizhevsky, Ilya Sutskever, and Geoffrey E Hinton. Imagenet classification with deep con-  
 613 volutional neural networks. In F. Pereira, C.J. Burges, L. Bottou, and K.Q. Weinberger, editors,  
 614 *Proceedings of Advances in Neural Information Processing Systems*, volume 25. Curran Asso-  
 615 ciates, Inc., 2012.

616 Ze Liu, Yutong Lin, Yue Cao, Han Hu, Yixuan Wei, Zheng Zhang, Stephen Lin, and Baining Guo.  
 617 Swin transformer: Hierarchical vision transformer using shifted windows. In *Proceedings of the*  
 618 *IEEE/CVF International Conference on Computer Vision (CVPR)*, pages 10012–10022, 2021.  
 619

620 Zhuang Liu, Hanzi Mao, Chao-Yuan Wu, Christoph Feichtenhofer, Trevor Darrell, and Saining Xie.  
 621 A convnet for the 2020s. In *Proceedings of the IEEE/CVF Conference on Computer Vision and*  
 622 *Pattern Recognition (CVPR)*, pages 11976–11986, 2022.

623 Cédric S Mesnage, Andrew Corbett, Jake Curry, Sareh Rowlands, Anjan Dutta, Richard Everson,  
 624 and Benno I Simmons. Copy-paste augmentation improves automatic species identification in  
 625 camera trap images. *Ecology and Evolution*, 15(11):e72357, 2025.

626 Emmanuel Moupojou, Appolinaire Tagne, Florent Retraint, Anicet Tadonkemwa, Dongmo Wilfried,  
 627 Hyppolite Tapamo, and Marcellin Nkenfack. Fieldplant: A dataset of field plant images for plant  
 628 disease detection and classification with deep learning. *IEEE Access*, 11:35398–35410, 2023.  
 629

630 Karl J. Niklas. The role of phyllotactic pattern as a “development constraint” on the interception of  
 631 light by leaf surfaces. *Evolution*, 42(1):1–16, 1988.

632 Renyong Pan, Jianwu Lin, Jitong Cai, Licai Zhang, Jiaming Liu, Xingtian Wen, Xiaoyulong Chen,  
 633 and Xin Zhang. A two-stage feature aggregation network for multi-category soybean leaf dis-  
 634 ease identification. *Journal of King Saud University-Computer and Information Sciences*, 35(8):  
 635 101669, 2023.

636 Tal Remez, Jonathan Huang, and Matthew Brown. Learning to segment via cut-and-paste. In  
 637 *Proceedings of the European conference on computer vision (ECCV)*, pages 37–52, 2018.  
 638

639 Wei-Hsiang Shen and Meng-Lin Li. Copy-paste image augmentation with poisson image editing for  
 640 ultrasound instance segmentation learning. In *Proceedings of the IEEE International Ultrasonics*  
 641 *Symposium (IUS)*, pages 1–3, 2023.

642 Sayali Shinde and Vahida Attar. MH-SoyaHealthVision: An indian UAV and leaf image dataset  
 643 for integrated crop health assessment, 2024. URL [https://data.mendeley.com/](https://data.mendeley.com/datasets/hkbgh5s3b7)  
 644 datasets/hkbgh5s3b7.  
 645

646 Karen Simonyan and Andrew Zisserman. Very deep convolutional networks for large-scale image  
 647 recognition. In *Proceedings of 3rd International Conference on Learning Representations (ICLR)*,  
 648 pages 1–14, 2015.

648 Davinder Singh, Naman Jain, Pranjali Jain, Pratik Kayal, Sudhakar Kumawat, and Nipun Batra.  
 649 Plantdoc: A dataset for visual plant disease detection. In *Proceedings of the 7th ACM IKDD*  
 650 *CoDS and 25th COMAD*, pages 249–253. 2020.

651

652 Sivm205. Soybean diseased leaf dataset, 2023. URL <https://www.kaggle.com/datasets/sivm205/soybean-diseased-leaf-dataset>.

653

654 Jianming Sun, Xuyao Hao, and Mengxin Zhao. Image recognition of soybean leaf disease based  
 655 on bilateral branching network bbn. In *Proceedings of the 2024 4th International Conference on*  
 656 *Bioinformatics and Intelligent Computing (BIC)*, pages 47–53, 2024a.

657

658 Yubing Sun, Lixin Ning, Bin Zhao, and Jun Yan. Tomato leaf disease classification by combining  
 659 efficientnetv2 and a swin transformer. *Applied Sciences*, 14(17), 2024b.

660

661 Christian Szegedy, Wei Liu, Yangqing Jia, Pierre Sermanet, Scott Reed, Dragomir Anguelov, Du-  
 662 mitru Erhan, Vincent Vanhoucke, and Andrew Rabinovich. Going deeper with convolutions. In  
 663 *Proceedings of the IEEE conference on computer vision and pattern recognition (CVPR)*, pages  
 664 1–9, 2015.

665

666 Jiemeng Tao, Peijian Cao, Yansong Xiao, Zhenhua Wang, Zhihua Huang, Jingjing Jin, Yongjun Liu,  
 667 Huaqun Yin, Tianbo Liu, and Zhicheng Zhou. Distribution of the potential pathogenic alternaria  
 668 on plant leaves determines foliar fungal communities around the disease spot. *Environmental Re-  
 search*, 200:111715, 2021. ISSN 0013-9351. doi: <https://doi.org/10.1016/j.envres.2021.111715>.

669

670 Everton Castelão Tetila, Bruno Brandoli Machado, Nícolas Alessandro Belete, David Augusto  
 671 Guimarães, and Hemerson Pistori. Identification of soybean foliar diseases using unmanned aerial  
 672 vehicle images. *IEEE Geoscience and Remote Sensing Letters*, 14(12):2190–2194, 2017.

673

674 Qilong Wang, Banggu Wu, Pengfei Zhu, Peihua Li, Wangmeng Zuo, and Qinghua Hu. Eca-net: Ef-  
 675 ficient channel attention for deep convolutional neural networks. In *Proceedings of the IEEE/CVF*  
 676 *Conference on Computer Vision and Pattern Recognition (CVPR)*, pages 11534–11542, 2020.

677

678 Daniel Ward, Peyman Moghadam, and Nicolas Hudson. Deep leaf segmentation using synthetic  
 679 data. *arXiv preprint arXiv:1807.10931*, 2018.

680

681 Sanghyun Woo, Jongchan Park, Joon-Young Lee, and In So Kweon. CBAM: Convolutional block  
 682 attention module. In *Proceedings of the European Conference on Computer Vision (ECCV)*,  
 683 *pages=3–19*, 2018.

684

685 Qinghai Wu, Xiao Ma, Haifeng Liu, Cunguang Bi, Helong Yu, Meijing Liang, Jicheng Zhang,  
 686 Qi Li, You Tang, and Guanshi Ye. A classification method for soybean leaf diseases based on an  
 687 improved convnext model. *Scientific Reports*, 13(1):19141, 2023.

688

689 XB Yang, JP Snow, and GT Berggren. Patterns of rhizoctonia foliar blight on soybean and effect of  
 690 aggregation on disease development. *Phytopathology*, 81(3):287–293, 1991.

691

692 Yang Yang, Dongni Mao, Hiroaki Santo, Yasuyuki Matsushita, and Fumio Okura. Neuraleaf: Neu-  
 693 ral parametric leaf models with shape and deformation disentanglement. In *Proceedings of the*  
 694 *IEEE/CVF International Conference on Computer Vision (ICCV)*, 2025.

695

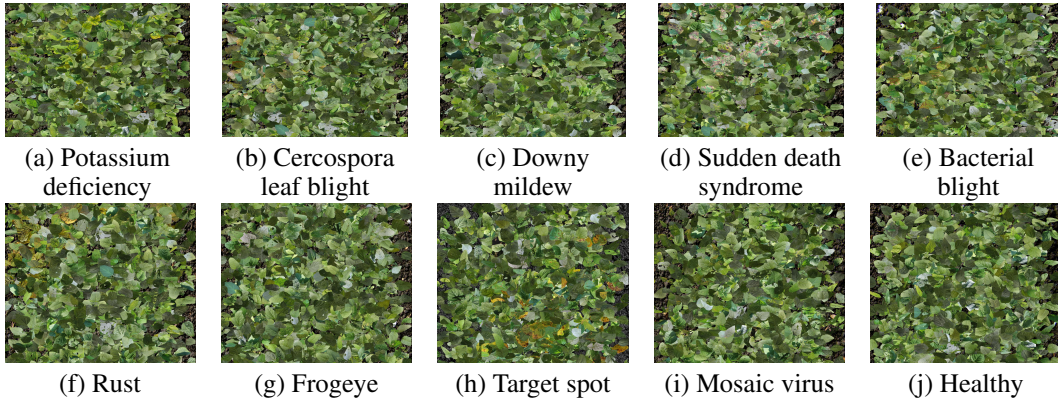
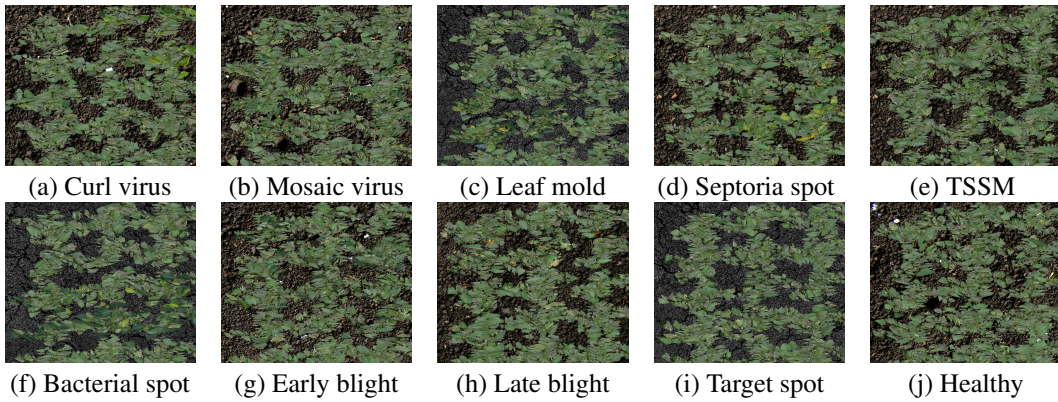
696 V Yogabalajee, Karthic Sundaram, and Kamaraj Kanagaraj. Soybean leaf disease classification  
 697 using enhanced densenet121. In *Proceedings of the 10th International Conference on Advanced*  
 698 *Computing and Communication Systems (ICACCS)*, volume 1, pages 1515–1520, 2024.

699

700 Xiao Yu, Qi Gong, Cong Chen, and Lina Lu. Automatic diagnosis of soybean leaf disease by transfer  
 701 learning. *American Journal of Biochemistry and Biotechnology*, 18(2):252–260, 2022.

## A APPENDIX

This section contains additional evidence to support our dataset and data generation method.

Figure 6: Generated soybean foliage images of 9 diseases, labeled by (a) to (i), for  $\gamma = 15\%$ .Figure 7: Generated tomato foliage images of 9 diseases, labeled by (a) to (i), for  $\gamma = 15\%$ .

### A.1 GENERATED FOLIAGE IMAGES

The generated diseased foliage images for both Soybean and Tomato are shown next.

### A.2 NATURAL FOLIAGE IMAGE

Foliagen is based on the observation of natural foliage and the findings given in published articles, to obtain high quality data for foliage disease classification. Our work evaluates MH-SoyaVisionHealth (Shinde and Attar, 2024), a natural soybean foliage dataset with 2 disease categories, rust and mosaic virus. Figure 8 depicts real-world soybean foliage images collected using UAVs at a farm in India.



Figure 8: Sample soybean foliage images from the MH-SoyaVisionHealth dataset (Shinde and Attar, 2024).

#### A.2.1 FOLIAGE GENERATION USING GENERATIVE MODEL

Recently, generative models have been used to generate almost all digital artifacts, including photos, videos, and texts. In the context of photos, the generative adversarial networks (GAN) and diffusion

models have been used extensively. Hence, we experiment with Deep Convolutional Generative Adversarial Network (DCGAN), Denoising Diffusion Probabilistic Model (DDPM), and PixelCNN to generate diseased foliage images from the real-world MH-SoyaVisionHealth dataset. All generative models are trained for 100 epochs before generating images from them, with their outcomes depicted in Figure 9.

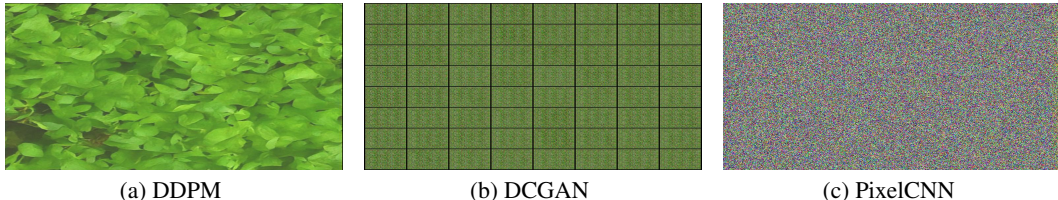


Figure 9: Foliage generated using generative models.

### A.3 ADDITIONAL EXPERIMENTAL RESULTS

We conducted extensive experimentation with multiple strategies aimed at strengthening the viability and reliability of our dataset. These efforts included (1) exploring alternative data preparation and augmentation techniques and (2) comparing the results of Foliagen with the baselines to ensure that its resulting dataset captures realistic variability while preserving essential pathological characteristics. The outcomes of these investigations are presented in the following sections.

#### A.3.1 TRANSFER LEARNING USING ASDID

The models were pre-trained on the raw ASDID dataset and then fine-tuned with 5% of the MH-SoyaVisionHealth dataset. Table 4 illustrates the transfer learning performance with all the hyper-parameters configured as discussed in Section 4.

Table 4: Comparative performance evaluation results (in %) under the MH-SoyaVisionHealth dataset, pre-trained on ASDID dataset

Models	Accuracy	F1-score	Precision	Recall
VGG19 (Simonyan and Zisserman, 2015)	33.33	32.56	33.33	32.94
ResNet50 (He et al., 2016)	<b>74.84</b>	<b>75.31</b>	<b>75.80</b>	<b>74.82</b>
DenseNet121 (Huang et al., 2017)	35.37	34.43	33.55	35.36
Swin Transformer (Liu et al., 2021)	69.45	69.92	70.38	69.45
CBAM-ConvNeXt (Wu et al., 2023)	49.32	50.25	51.22	49.32

#### A.3.2 VARYING LEAF SIZES

The current version of the dataset reduces the size of individual leaves to a similar size as that of natural foliage leaves. This step gave a huge performance hike in the evaluated model. Many variations in leaf sizes, maintaining their aspect ratio, were used to create the dataset and were evaluated. One of the experimental results is shown in Table 5. It is vivid from the table that upscaling the leaf size leads to degraded performance for all classifiers; this is also true when the leaves are downscaled in size.

#### A.3.3 COMPARISON OF MODEL METRICS

Foliagen, as demonstrated by the results in this paper, generates high-quality datasets for foliage disease classification in both soybean and tomato. Besides accuracy, computational efficiency is also important for consideration. Table 6 reports the model parameter count and the per-epoch training times when trained on a generated foliage dataset, compared with those of the baseline constructed from individual leaf images. As expected, single-leaf images incur lower training times per epoch due to their reduced visual complexity. Despite their substantially higher image complexity and larger spatial dimensions, foliage images are subject to only some 30% increases in per-epoch

810  
 811 Table 5: Comparative performance evaluation results (in %) under the generated tomato foliage  
 812 image dataset with  $2 \times$  upscaled leaf size

813 <b>Models</b>	814 <b>Accuracy</b>	815 <b>F1-score</b>	816 <b>Precision</b>	817 <b>Recall</b>
VGG19 (Simonyan and Zisserman, 2015)	65.23	65.41	65.59	65.23
ResNet50 (He et al., 2016)	76.73	77.61	78.51	76.73
DenseNet121 (Huang et al., 2017)	<b>83.78</b>	<b>83.14</b>	<b>82.38</b>	<b>83.92</b>
Swin Transformer (Liu et al., 2021)	67.95	68.96	70.02	67.91
CBAM-ConvNeXt (Wu et al., 2023)	71.88	71.96	72.03	71.88

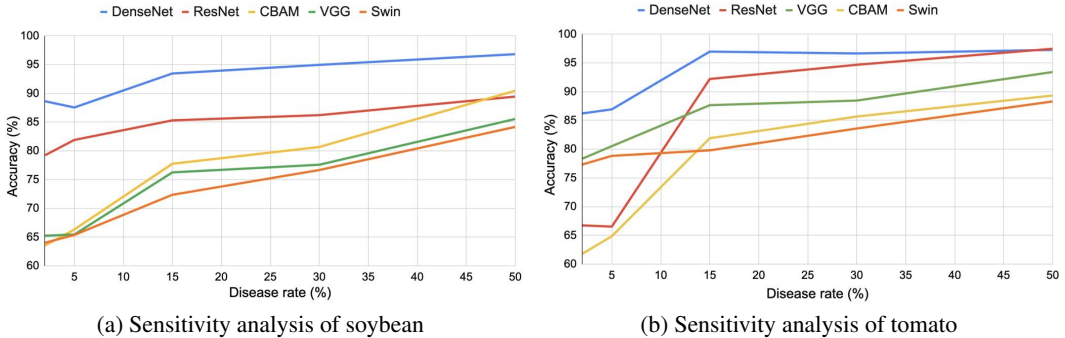
820 training time, indicating that Foliagen produces results to train useful classifiers for real-world  
 821 applications, with acceptable computational overheads.

822  
 823 Table 6: Comparative model evaluation metrics results under the generated dataset and the single-  
 824 leaf image datasets of Soybean

825 <b>Models</b>	826 <b>For generated dataset (<math>\gamma = 15\%</math>)</b>		827 <b>For single leaf images</b>	
	828 <b>No. of Parameters</b>	829 <b>Per epoch training time</b>	830 <b>No. of Parameters</b>	831 <b>Per epoch training time</b>
VGG19 (Simonyan and Zisserman, 2015)	139,611,210	459.17	139,611,210	331.03
ResNet50 (He et al., 2016)	23,581,642	433.38	23,581,642	244.10
DenseNet121 (Huang et al., 2017)	7,047,754	454.73	7,047,754	645.819
Swin Transformer (Liu et al., 2021)	27,527,044	419.10	27,527,044	290.10
CBAM-ConvNeXt (Liu et al., 2021)	29,727,934	437.34	29,727,934	331.03

#### 832 A.4 SENSITIVITY ANALYSIS OF DISEASE RATE

833 Figure 10 illustrates the sensitivity analytic results across disease rates, revealing consistent per-  
 834 formance patterns among the classifiers. Accuracy increases for all models as disease prevalence  
 835 intensifies, with DenseNet maintaining the highest and most stable performance levels across the  
 836 full disease rate range and ResNet showing a similarly smooth upward trend. VGG improves more  
 837 gradually, becoming competitive only at higher disease rates, whereas CBAM remains highly sen-  
 838 sitive to disease severity, performing poorly at low levels but rising sharply once pathological cues  
 839 become pronounced. Swin consistently yields the weakest performance with limited benefit from  
 840 increased disease information.



852 Figure 10: Sensitivity analysis on the disease rate for soybean and tomato.

#### 853 A.5 ABLATION STUDY

854 To investigate the contribution of each component of the Foliagen framework, we conducted an  
 855 extensive ablation study on both soybean and tomato plants. Table 7 reports the performance of  
 856 different framework variants for both crops. Specifically, we evaluate two configurations: (1) with-  
 857 out the plant-level component, where naturally structured single-plant foliage is generated solely by  
 858 arranging leaves according to the spiral phyllotactic pattern, and (2) without removing background  
 859 from individual leaf images. The results clearly demonstrate that the full Foliagen framework con-  
 860 sistsently outperforms all ablated variants across all evaluated models. As expected, retaining the  
 861

864 background in leaf images leads to a substantial performance drop, highlighting the importance of  
 865 clean leaf segmentation for realistic foliage synthesis.  
 866

867  
868 **Table 7: Ablation study of Foliagen for Soybean and Tomato ( $\gamma = 15\%$ )**

869 Models	870 <b>Soybean</b>			871 <b>Tomato</b>		
	872 <b>Ours</b>	873 <b>Without plant level</b>	874 <b>With background</b>	875 <b>Ours</b>	876 <b>Without plant level</b>	877 <b>With background</b>
VGG19	<b>76.26</b>	69.29	37.52	<b>87.66</b>	82.60	53.71
ResNet50	<b>85.31</b>	82.01	45.78	<b>92.22</b>	87.39	55.32
DenseNet121	<b>91.47</b>	84.66	76.66	<b>96.98</b>	90.32	71.63
Swin Transformer	<b>72.36</b>	65.94	32.58	<b>79.80</b>	66.53	43.84
CBAM-ConvNeXt	<b>77.76</b>	73.15	49.15	<b>81.91</b>	72.51	59.50

878  
879 **A.6 CONFIGURATION FILE**

880 As depicted in Figure 3, all level of foliage generation require plant specific information to generate  
 881 high quality foliage images. The configuration file includes number of leaves, disease rate, and other  
 882 factors listed next.

```
883 {
 884   "num_leaves": 50,
 885   "diseases": "list_of_diseases",
 886   "foliage_size": "(1024, 1500)",
 887   "single_plant_size": 512,
 888   "single_leaf_size": 70,
 889   "num_plants": 16,
 890   "plant_offset": 100,
 891   "disease_rate": 15,
 892   "background_image_path": "<path_to_background_images>",
 893   "input_path": "<path_to_raw_input_images>",
 894   "output_path": "<path_to_save_generated_images>",
 895   "type": "tomato",
 896   "leaf_spacing": 60
 897 }
```

898  
899  
900  
901  
902  
903  
904  
905  
906  
907  
908  
909  
910  
911  
912  
913  
914  
915  
916  
917